

Solid State Synthesis and Properties of Relaxor (1-x)BKT - xBNZ Ceramics

Espen Tjønneland Wefring, Maxim I. Morozov, Mari-Ann Einarsrud, Tor Grande*

Department of Materials Science and Engineering, Norwegian University of Science and Technology, N-7491 Trondheim, Norway

Conventional solid state synthesis was used to synthesize dense and phase pure ceramics in the $(1-x)\text{Bi}_{0.5}\text{K}_{0.5}\text{TiO}_3 - x\text{Bi}_{0.5}\text{Na}_{0.5}\text{ZrO}_3$ (BKT-BNZ) system. Structural characterization was done using X-ray diffraction at both room temperature and elevated temperatures, identifying a transition from tetragonal $x\text{Bi}_{0.5}\text{Na}_{0.5}\text{ZrO}_3$ (xBNZ, $x=0-0.10$) to cubic xBNZ for $x=0.15-0.80$. Dielectric properties were investigated with respect to both temperature (RT - 600°C) and frequency ($1-10^6$ Hz). Relaxor-like behavior was retained for all the materials investigated, evident by the broadening of the relative dielectric permittivity peaks at transition temperatures as well as frequency dispersion at their maximum. The maximum dielectric constant at elevated temperature was found for 0.15BNZ. Electric field induced strain and polarization response was also investigated for several compositions at RT and the largest field induced strain was observed for the 0.10BNZ ceramics. The composition range with best performance coincides with the transition from tetragonal to ~~pseudo~~ cubic crystal structure.

I. Introduction

Development of lead-free piezoelectric ceramics has attained significant attention in recent years.¹ There is a need to replace the state of the art lead containing piezoceramics such as $\text{Pb}(\text{Zr}_{1-x}\text{Ti}_x)\text{O}_3$ (PZT) with lead-free alternatives due to environmental concerns. Amongst others, the European Union has passed legislations limiting the amount of lead in electronics, with the exception of piezoelectrics until lead-free alternatives are available.^{1,2}

Two of the lead-free alternatives to PZT are $\text{Bi}_{0.5}\text{K}_{0.5}\text{TiO}_3$ (BKT) and $\text{Bi}_{0.5}\text{Na}_{0.5}\text{TiO}_3$ (BNT). Both BKT and BNT, as well as their solid solution have been intensively studied.³⁻¹¹ Other lead-free systems based on BKT or BNT, such as $\text{BKT-Bi}_{0.5}\text{K}_{0.5}\text{ZrO}_3$ ¹² (BKT-BKZ), BKT-BiFeO_3 ^{13,14} (BKT-BFO), BKT-BaTiO_3 ¹⁵ (BKT-BT), $\text{BKT-K}_{0.5}\text{Na}_{0.5}\text{NbO}_3$ ¹⁶ (BKT-KNN), BKT-BiScO_3 ¹⁷ (BKT-BS), BNT-BaTiO_3 ¹⁸, $\text{BNT-K}_{0.5}\text{Na}_{0.5}\text{NbO}_3$ ¹⁹ and BNT-NaNbO_3 ²⁰ have also been investigated.

*Corresponding author, Tel/fax: +47 73594002/73550203
Email address: ~~tor~~-grande@ntnu.no (Tor Grande)

~~BKT is a tetragonal ferroelectric at room temperature.~~ It transforms to a pseudo cubic crystal structure around 300°C (T_2) ~~giving it~~ relaxor properties and finally it becomes cubic and paraelectric above 380°C.^{3-5,8} BNT is a ferroelectric relaxor, which shows a gradual phase transition from RT rhombohedral (R3c) to tetragonal crystal structure between 200°C and 320°C.^{6,7} It has been suggested that the transition from tetragonal to cubic phase does not occur until 620°C.⁷

Separate studies have been conducted on BKT and BNT where Ti is replaced with Zr. The tetragonality of BKT has been found to prevail up to 5-11 mol% substitution of Zr for Ti^{12,21} whereas pure $\text{Bi}_{0.5}\text{K}_{0.5}\text{ZrO}_3$ (BKZ) is found to be cubic $\text{Pm}\bar{3}\text{m}$ (IC~~nr.~~ 057-0823). A transition from rhombohedral to orthorhombic structure has been observed for BNT upon 58-60 mol% substitution of Zr for Ti.²¹⁻²³ The crystal structure of $\text{Bi}_{0.5}\text{Na}_{0.5}\text{ZrO}_3$ (BNZ) has been reported to be orthorhombic Pnma .²⁴

The effect of Zr substitution ~~for Ti~~ on the piezoelectric and dielectric properties of BNT and BKT has not been reported to a large extent. A slight increase of the dielectric constant (ϵ') with 5-10 mol% substitution of Zr for Ti in BKT and BNT has been observed.^{21,25} The piezoelectric coefficient (d_{33}) has been found to decrease from 68 pC/N to 40 pC/N when substituting 20 mol% Zr for Ti in BNT.²⁵

Compositions near a morphotropic phase boundary (MPB) in a solid solution of two or more compounds are known to give enhanced piezoelectric properties, as in PZT where the MPB is found at a Zr:Ti ratio corresponding to 52:48.²⁶ An MPB in the systems BKT-BNT ~~and BNT-BT~~ has been reported at 16-20 mol% BKT ~~and 6mol% BT, respectively.~~^{11,18} A general decrease of the transition temperatures relative to pure BNT is observed at ~~the MPB in BKT-BNT this composition,~~ in addition to increased piezoelectric properties relative to both end members.^{10,11} ~~The MPB in the above mentioned materials is found in the composition region where the symmetry changes from tetragonal to rhombohedral.~~²⁶ Although the symmetry of the end members in the present study is orthorhombic (BNZ) and tetragonal (BKT), a BKT-BNZ solid solution could possibly involve an MPB or similar phenomena such as a "morphotropic phase".^{1,27} No MPB has been reported close to pure BKT.

Here we report on the solid state synthesis and structural, dielectric and piezoelectric properties of the (1-x)BKT-xBNZ materials system, which have not been reported on previously although BNZ was suggested as a ferroelectric already in 1961.⁹ Both the large difference in tolerance factor (~~$t_{\text{BNZ}} = 0.89$, $t_{\text{BKT}} = 0.99$~~) and the ~~different tetragonal (BKT) and orthorhombic (BNZ)~~ symmetry of the end members suggest a possible MPB along the BKT-BNZ composition line.

II. Experimental

A conventional solid state synthesis route was used to obtain dense ceramic samples of the composition $(1-x)\text{BKT} - x\text{BNZ}$ with $x=0, 0.05, 0.10, 0.15, 0.20, 0.30, 0.40$ and 0.50 . Ceramics with $x=0.60, 0.70, 0.80, 0.90$ and 1 were also prepared, but without sufficient density or phase purity. The precursors, Bi_2O_3 (Aldrich, 99.9%), TiO_2 (Aldrich, 99.9%), ZrO_2 (Tosoh), Na_2CO_3 (Aldrich, 99.99%) and K_2CO_3 (Aldrich, 99.99%) were first dried ~~195°C~~ in a vacuum furnace ~~for~~ (195°C, ~12 h). Stoichiometric amounts of precursors were mixed and ball milled ~~for~~ (24 h, in isopropanol) using 5 mm yttrium stabilized ZrO_2 balls. Prior to this, ZrO_2 was ball milled by the same procedure, but separately, to break down ZrO_2 agglomerates. The calcination temperature was optimised for all compositions ranging from 700°C to 750°C, and the calcined powders were ball milled by the same procedure as the precursor mixture. The calcined powders were dried and sieved (250 μm sieve). Pellets (10 mm diameter) were prepared using uniaxial pressing (50 MPa - 100 MPa) followed by cold isostatic pressing (200 MPa). The sintering temperature and time was optimized for all compositions to produce dense and phase pure ceramics. The pellets were surrounded with sacrificial powder inside an alumina crucible closed with a lid during sintering. Detailed calcination and sintering programs for each composition are summarized in Table 1.

~~The relative density was taken as the ratio between the absolute density of the pellets, measured by Archimedes method (ISO 5017:1998(E)), and the theoretical density, calculated from lattice parameters determined as described below. and relative density was calculated based on theoretical density calculated from lattice parameters found by Pawley refinement of XRD data.~~

Crystal structure was studied using x-ray diffraction (XRD; Model D5005 diffractometer with $\text{CuK}\alpha$ -radiation and secondary monochromator, Siemens). The diffractograms were obtained from crushed sintered pellets annealed at 600°C for 12 h to relieve mechanical stresses introduced during crushing (no annealing was performed prior to XRD of $x=0.9$ and $x=1.0$). Lattice parameters of the investigated compositions were determined by Pawley refinement using the Topas software for $0 \leq x \leq 10.80$.²⁸ High temperature XRD (HTXRD; Bruker D8Advance with an mri high temperature camera) up to 600°C ~~was done on BKT ($x=0$) powder.~~

The microstructure of fabricated ceramics was studied by scanning electron microscopy (SEM; Hitachi S-3400N). Pellets were polished, thermally etched and coated with carbon. The grain size was measured by the intercept method, measuring ~30 grains for each sample. ~~at temperatures 50°C - 100°C below their sintering temperature and coated with carbon to ensure sufficient surface conductivity.~~ The chemical composition of the samples was investigated using energy-dispersive x-ray spectroscopy (EDS; X-MAX, Oxford Instruments).

The piezoelectric and dielectric characterization was performed using samples with $\geq 96\%$ density. The samples were polished with grade #1200 silicon carbide grinding paper to thicknesses from 0.69 to 2.32 mm. Electrodes were applied on the pellet faces prior to electrical testing. A spray on silver electrode (Doduco) was used for RT piezoelectric testing, ~~and the electrode was~~ (cured at 200°C, 12 h). ~~Sputtered~~ ~~g~~Gold electrodes were ~~used for sputtered onto pellets for~~ dielectric measurements at elevated temperatures.

Dielectric properties were characterized using a frequency analyzer (Alpha-A High Performance Frequency Analyzer, Novocontrol Technologies) connected to a heating unit (for $0.30 \leq x \leq 0.50$: combined furnace and electrode setup, Novotherm, Novocontrol Technologies; for $0 \leq x \leq 0.20$: tubular furnace with Probostat, NorECs). All samples (both for dielectric and piezoelectric testing) were subject to a RT-scan at frequencies 10^7 Hz - 10^{-2} Hz to confirm sufficient sample quality before further characterization. Two samples of each composition were initially tested and the sample with the lowest loss tangent was used for the piezoelectric measurements.

Dielectric spectroscopy at elevated temperatures (RT - 600°C) was performed with constant heating rate of (2°C/min) and a measurement was done every 30 seconds at frequencies 1- 10^6 Hz ~~with 1V (AC).~~ ~~A voltage of 1 V (AC) was applied across the sample during measurements.~~

Piezoelectric properties were determined by studying the electric field-induced polarization and strain response of the samples at RT, with the samples submerged in silicone fluid (Wacker AK 100), using an aixPES - Piezoelectric Evaluation System (aixACCT). All samples were subject to bipolar measurements with subsequent unipolar measurements at a constant frequency of (0.25 Hz). Dielectric breakdown was typically observed ~~for as the electric fields was increased~~ above 60 kV/cm.

III. Results

Dense ~~and phase pure~~ ceramics in the composition region $0 \leq x \leq 0.50$ were successfully prepared by the conventional solid state synthesis method. The calcination and sintering temperatures were optimized for all compositions and densities $\geq 96\%$ were subsequently obtained ~~for $0 \leq x \leq 0.50$~~ as summarized in Table 1.

X-ray diffractograms of powder samples ~~in the 2θ range $20^\circ - 60^\circ$~~ are shown in Figure 1 (~~$2\theta = 20^\circ - 60^\circ$~~). The reflections can be indexed to the tetragonal or the cubic perovskite crystal structure for $x \leq 0.8$. The reflections shift to lower 2θ angles as the BNZ content increases, demonstrating an increasing size of the unit cell with increasing BNZ content. ~~The increasing unit cell volume growing unit cell~~ is confirmed by the unit cell parameters determined by Pawley refinement, as shown in Figure 2 and listed in Table 2. The unit cell of xBNZ ($x=0-0.10$) was refined using the tetragonal P4mm symmetry, in accordance with what is

reported for BKT.⁸ The diffractograms were refined using cubic $Pm\bar{3}m$ unit cell for x BNZ ($x=0.15-0.80$), while BNZ ($x=1$) was refined using the orthorhombic $Pnma$ unit cell ~~in accordance with what has been reported previously.~~²⁴ ~~At high BKT content no secondary phases could be observed by XRD, but from $x=0.2$ traces of secondary phases could be observed It should be noted that the diffractograms used to determine cell parameters for $x \geq 0.60$ (not shown in Figure 1) were obtained from samples, which were not phase pure.~~ The ceramics of $x=0.80$ and $x=1$ contained a secondary phase suggested to be $Bi_2Zr_2O_7$ based on findings by EDS.²⁹

Selected HTXRD diffractograms for ~~BKT ($x=0$)~~ up to 600°C are shown in Figure 3. The tetragonal splitting of the $(100)_{pc}$ diffraction line gradually vanishes and the tetragonal splitting is not possible to identify above 300°C in line with previous reports.³⁰

The final density and grain size of the ceramics is summarized ~~The densities and grain sizes for the composition range $0 \leq x \leq 0.50$ are included~~ in Table 1. The grain size increased slowly from $x=0$ to $x=0.30$ before a significant increase was seen for $x=0.40$ and $x=0.50$. SEM micrographs of the thermally etched pellets are presented in Figure 4, demonstrating the significant grain size increase observed for $x=0.50$. ~~The micrographs also show a not homogeneous grain size and some exaggerated grain growth.~~ The nominal chemical composition of all the compositions was confirmed by EDS.

The variation of the relative dielectric permittivity, ϵ' , was investigated for $0 \leq x \leq 0.50$ with respect to temperature and frequency. Figure 5a shows how ϵ' varies with temperature at 10 kHz. The ϵ' maximum (ϵ'_{max}) becomes less pronounced as the BNZ content exceed 15 mol% ($x=0.15$), and for $x=0.40$ and $x=0.50$ it is difficult to establish the temperature at the maximum. The temperature of maximum relative permittivity (T_m) decreases with increasing BNZ content and $x=0.15$ displays the highest ϵ' of 3507 at 265°C (10 kHz). The maximum value of ϵ' is given in Table 2, together with ~~T_m the corresponding temperature.~~

The frequency dependence of ϵ' vs. temperature for $x=0.15$ is shown in Figure 5b. Relaxor type behavior is evident by the significant shift in ϵ' with frequency. The same behavior was observed for all compositions investigated. The room temperature ϵ' and dielectric losses as a function of frequency and composition for the samples used to characterize the piezoelectric properties are shown in Figure 6.

The polarization vs. applied electric field curves for $0 \leq x \leq 0.50$ compositions ~~recorded during cycling with bipolar electric field at RF (0.25 Hz)~~ are displayed in Figure 7a and Figure 7b. The maximum polarization (P_{max}) was obtained for the $x=0.10$ composition with $20.5 \mu\text{C}/\text{cm}^2$ at 60 kV/cm. The ~~qualitative~~ shape of the hysteresis loop did not depend on the maximum electric field in the range 25-60kV/cm. The polarization decreased significantly and the hysteresis loop became gradually more closed as ~~the $x \rightarrow 0.50$ composition is approached.~~ with $P_{max}=4.4 \mu\text{C}/\text{cm}^2$ at 60kV/cm for $x=0.50$ ~~The highest~~

polarization obtained for $x=0.50$ was $4.4 \mu\text{C}/\text{cm}^2$ at $60\text{kV}/\text{cm}$. The same trend was also apparent in strain vs. electric field curves shown in Figure 7c and Figure 7d. The highest strain ($S_{max,b}$) obtained was 0.08 % for $x=0.1$. Following the reduced polarization at increasing BNZ content, the strain was also significantly reduced. P_{max} and $S_{max,b}$ The highest polarization and strain obtained for all compositions are included in Table 2. Table 2 also shows the unipolar electric field induced strain of the investigated compositions where $S_{max,u}$ is the maximum obtained strain (with remanent strain subtracted) and E_{max} is the maximum applied electric field.


IV. Discussion

The dielectric and piezoelectric properties reported in this work for xBNZ ($x=0-0.50$) demonstrated a peak in performance for $x=0.15$ and $x=0.10$, respectively. The compositions corresponding to maximum performance coincide with the transition from tetragonal to cubic symmetry (Figure 2). We have calculated the Goldschmidt tolerance factor, t , for the different compositions using the Shannon radii³¹ with A and B cations of coordination number (CN) 12 and 6, respectively. For Bi CN=8 was used, giving a tolerance factor for the present end members of 0.99 (BKT) and 0.89 (BNZ). The Goldschmidt tolerance factor, t of the $x=0.10$ is 0.98. Investigations of other BKT-based materials systems reveal that BKT loses its tetragonality at $t \approx 0.96-0.98$ when substituting with BKZ^{12,21}, BFO¹³, KNN¹⁶, BS¹⁷ and BNT^{11,32,33} (all t based on Shannon radii³¹). There is currently no consensus on the exact composition where the transition from tetragonal symmetry occurs in the BKT-BNT system.³³ A tentative structural phase diagram of the ternary reciprocal system BKT-BNZ is shown in Figure 8. This is based on the present data obtained in this study and combined with reported literature data.^{11,12,21,32-34} The diagram shows a dominating large cubic/pseudo cubic region suggesting that large amounts of substitution in the BKT-BNZ system is not beneficial. The tetragonal area of BKT is mainly largely constrained to the Ti-rich region of the diagram. This is the region with higher tolerance factor and corresponds to the t -range given above for which BKT loses its tetragonality. Based on the current knowledge it could be predicted that the loss of tetragonality would occur at $x \sim 0.10$ along the $(1-x)\text{BKT} - x\text{BNZ}$ composition joint. This transition however does not show the characteristics of being an MPB as the tetragonal and orthorhombic phase regions are separated by a large area with cubic symmetry.

Figure 5b shows that T_m is a function of frequency for the $x=0.15$ ceramics. The same was observed for all the other compositions investigated. The broad temperature and frequency dependence of ϵ' is typical of relaxor materials. However, our data are not sufficient to attribute the investigated materials to any specific class of relaxors (see e.g. Bokov and Ye³⁵), hence relaxor-like is used. Relaxor-like behavior was

maintained for all levels of BNZ substitution. The same has been observed when substituting BKT with BKZ, BS and BFO.^{12,14,17} The dielectric dispersion increases as the BNZ content is increased along with the general decrease of ϵ' and T_m . These trends are most likely related to the structural development with composition ~~which we discuss later.~~

RT dielectric constants of the ternary reciprocal BKT-BNZ materials system are summarized in Figure 9. ϵ'_{RT} for BKT (x=0) correspond to ~~previously measured~~ data (450-720).^{5,12,32,36,37} It is apparent from the contour plot that the Ti rich compositions exhibit the highest dielectric constants, and that addition of large amounts of Zr in general suppresses ϵ'_{RT} . The maximum ϵ'_{RT} observed for the BKT-BNT system is found near the MPB at ~20 mol% BKT in BNT.^{10,32} A 15 mol% substitution of BNZ to BKT is currently the second best composition investigated in the ternary reciprocal BKT-BNZ system at RT.

~~ϵ'_{RT} of the composition showing the highest ϵ' at T_m in the BKT-BNZ system and other BKT-based solid solutions have been compared.~~ Solid solutions of BKT-BNT (80% BNT), BKT-BFO (25% BFO), BKT-BNZ (15% BNZ) and BKT-BS (15% BS) all show similar ϵ'_{RT} , which is higher than the ϵ'_{RT} of the end members.  The BKT-KNN and BKT-BKZ systems do not show any increase of the maximum ϵ' at elevated temperatures relative to BKT (x=0) and are hence not seen as a viable alternative to improve the properties of BKT. At elevated temperatures the BKT-BNT and BKT-BFO solid solutions show an ϵ' 2-3 times higher than what is observed for BKT-BNZ and BKT-BS.^{10,12,14,16,17}

The relaxor behavior observed above ~300°C for BKT (x=0) is in accordance with earlier reports.^{12,17} Full width-half maximum (FWHM) values of selected diffraction lines from the ~~high temperature~~HTXRD experiment performed on BKT (x=0, Figure 3) are shown in Figure 10a). The data show an abrupt drop of FWHM near 300°C in agreement with where T_2 has been reported earlier followed by a more gradual decrease as the temperature rises to ~400°C.^{3,8,30} The region between ~300°C and ~400°C is the pseudo cubic region of BKT where the relaxor behavior is observed. ~~Relaxor-like behavior was maintained as the BNZ content was increased showing frequency dispersion of ϵ' with temperature. The same has been observed when substituting BKT with BKZ, BS and BFO.^{12,14,17} The dielectric dispersion increases as the BNZ content is increased along with the general decrease of ϵ' and T_m . These trends are most likely related to the structural development with composition as discussed further below.~~

The ~~polarization and strain response to the applied electric field of BKT (x=0) in this study is within the range of what has been observed elsewhere.~~^{17,37} The increase of polarization and strain response is though much lower than what has been obtained both for the BKT-BFO and BKT-BNT systems.^{10,13,14} The reduced opening of the hysteresis loops as x increases ~~as more BNZ is added to BKT~~ is attributed to the increasingly cubic character of the material. ~~Other solid solutions such as BKT-BFO also show reduced~~

opening, but this is probably related to domain pinning, is also observed when adding BKT to BFO, and may occur due to various domain pinning mechanisms observed in ferroelectrics.^{1,13} Another factor to consider is that the average size of the A-site cation decreases while the average size of the B-site cation increases as more BNZ is added to BKT. This reduces the tolerance factor and the structure adapts by tilting the BO₆ octahedra (BNZ is orthorhombic due to octahedral tilting). This also reduces the structures ability to accommodate the ferroelectric displacement of Ti⁴⁺ which consequently reduces the overall ferroelectric response of the material.³⁸ Another factor to consider is the ratio between unit cell size and the average size of the cations. As the amount of BNZ increases the size of the unit cell increases (Figure 2), but the relative size of the B-cation increases more. The average size of the B-cation increases 19% (the size of the A-cation decreases 12%). The crystal lattice adapts to this by tilting the BO₆ octahedra resulting in less space available to accommodate polarization. A study of the local atomic structure of BKT-BNT showed that as the Na content increased the displacement of Ti decreased. This was attributed to the reduced unit cell parameters observed for the Na-rich compositions. Combined with shorter Bi-Ti distances and an increasing B-cation size, the above mentioned space limitation is a probable reason for the reduced polarization and strain response observed in BKT-BNZ.³⁸

By examining the strain response of $0 \leq x \leq 0.50$ ceramics (Figure 7c and Figure 7d) it is apparent that the response becomes more electrostrictive as x increases, identified by the transition from ferroelectric butterfly loops to almost parabolic strain-electric field curves. electrostriction shows an increasingly dominating role over piezoelectric strain response. The strain response of a material is a combination of piezoelectric effect and electrostriction. All dielectric materials show electrostriction, whereas piezoelectricity is only observed in materials of a non-centrosymmetric space group. In short it can be described using Equation 1:

$$S_i = g_{ij}P_j + Q_{ij}P_j^2 \quad (1)$$

where S is the total strain, g is the piezoelectric coefficient, P is the polarization, Q is the electrostriction coefficient and i,j (=1,2,3) are directional indexes.¹ Due to the square dependency of electrostrictive strain on polarization it is clear that electrostriction can only produce positive strain, and a plot of S vs P² will show a linear relationship. This is very close to what is observed for x=0.50 (figure not shown). The domain structure of the pseudo cubic phase observed for $0.15 \leq x \leq 0.580$ is probably a combination of a cubic matrix phase with embedded local polar nanodomains. These polar domains will provide piezoelectric response in an inherently cubic centrosymmetric matrix phase.³⁵ The nanodomains will disappear gradually as x increases and will eventually vanish completely, leaving behind a cubic paraelectric state where only electrostriction can be observed. The same gradual microstructural changes are observed as BKT (x=0) is heated from RT to above T_C where disappearance of the ferroelectric domains occur gradually between

280°C and 450°C.³⁰ Tetragonal to pseudo cubic transition has also been suggested for BKT-BNT³⁹ (as referred by³³), BKT-BKZ¹², BKT-BFO¹³ and BKT-BS¹⁷ solid solutions when moving away from the BKT rich region.

The P-E loops in Figure 7a and Figure 7b show a limited degree of saturation **with some evidence of non-ferroelectric contributions due to dielectric loss at high fields. These losses will manifest as an overestimation of the polarization (Table 2) but does not alter the observed trend between compositions.** Measurements of polarization vs. electric field strength were normally stopped at fields of 60kV/cm as higher fields typically gave electric breakdown. One sample (x=0.05) was though exposed to 70kV/cm and one (x=0.10) was exposed to 80kV/cm without any significant change of the hysteresis loop. As the coercive field of BKT is ~50kV/cm and the tetragonality is reduced with increasing BNZ content it is **proposed**~~believed~~ that the applied fields are sufficient to make the data relevant.^{5,40} It should be noted that the increasing polarization observed with increasing BKT content is not a manifestation of losses.⁴¹ There is no systematic indication when examining the dielectric loss of samples used for piezoelectric characterization that the observed polarization is manifestation of conductivity rather than real polarization, see Figure 6.

The FWHM of two x-ray diffraction lines is shown as a function of xBNZ in Figure 10b). Both these diffraction lines show tetragonal splitting at ambient temperatures for pure BKT. A drop of FWHM is, as expected, observed at x=0.10 where the transition from tetragonal to pseudo cubic crystal structure occur. The increase of FWHM at x=0.15 may be due to the polar nanodomains distributed throughout the cubic matrix phase. It is possible that these nanodomains introduce non-uniform stresses that may act to disturb the long range order seen by the x-rays and cause a "size effect" giving peak broadening. As the nanodomains gradually disappear, the "size effect" diminishes and the FWHM decrease down to a close to constant level at x=0.50-0.80. **It is also possible that there is a symmetry change for this composition that was not resolved by the XRD analysis, offering an alternative explanation to the broadening between x=0.15 and x=0.40.**

It has been noted by others that densification of BKT during sintering is difficult and hot pressing has been suggested as one measure to overcome this.^{5,37} Problems were not observed with respect to sinterability of BKT (x=0) in this work. A study was conducted to first find the lowest calcination temperature which gave a pure perovskite phase. A subsequent milling step was performed to obtain small particles, resulting in a higher driving force for densification during sintering. The resulting microstructure shows grain sizes similar to what has been reported elsewhere.^{4,5} The grain size increases gradually for $0 \leq x \leq 0.30$ and then increases significantly for x=0.40 and x=0.50. As x increases from 0, the ratio of the alkali precursors K_2CO_3 and Na_2CO_3 approach their eutectic composition at 55-58 mol% Na_2CO_3 and the liquidus temperature of

this carbonate mixture hence decreases with increasing BNZ content.⁴² The liquidus temperature of the $K_2CO_3 : Na_2CO_3$ ratio in the precursor mixture for $x=0.40$ and $x=0.50$ is $746^\circ C$ and $719^\circ C$, respectively. ~~The calcination temperature of $x=0.40$ and $x=0.50$ was $750^\circ C$,~~ showing that the two materials, ~~when calcined at $750^\circ C$,~~ were made in the presence of a transient liquid, not as a purely solid state synthesis. Such synthesis conditions allow for much higher ion mobility and may result in significant grain growth during calcination. The solidus and liquidus temperature of the carbonates in the precursor mixture for $x=0.30$ is $750^\circ C$ and $783^\circ C$, respectively, and hence only a very small amount of liquid can be expected at this composition and less grain growth is observed.⁴²

Based on experimental results ~~(not shown)~~ it is proposed that the transition from pseudo cubic to orthorhombic symmetry of the $(1-x)BKT - xBNZ$ system occurs at $0.80 \leq x \leq 0.90$ as ~~an~~ orthorhombic superstructure reflections ~~were was~~ observed ~~forat~~ $x=0.90$. This transition range also corresponds to a similar tolerance factor to that of the rhombohedral - orthorhombic transition of BNT-BNZ. ~~The dielectric and piezoelectric properties of $x=0.60-1.0$ were not studied in detail due to the low response observed for $x=0.5$ and the challenge to prepare materials with sufficient quality. Dielectric and piezoelectric characterization of $x=0.60-1.0$ compositions was not performed due to problems with obtaining ceramic samples of sufficient density and phase purity. Typically a sintering temperature gave a phase pure pellet at a given temperature ($850^\circ C - 900^\circ C$) but not sufficient density. Increasing the temperature to improve density led to growth of a secondary phase suggested to be $Bi_2Zr_2O_7$. For $x=0.90$ and 1.0 , no phase pure samples could be prepared by the present synthesis route.~~

V. Conclusion

Dense and phase pure materials of the composition $(1-x)Bi_{0.5}K_{0.5}TiO_3 - xBi_{0.5}Na_{0.5}ZrO_3$ ~~($x=0-0.50$)~~ were fabricated using conventional solid state synthesis. The route gave dense and fine-grained ceramics, also for pure BKT. The crystal structure was found to be tetragonal for $0 \leq x \leq 0.10$ and pseudo cubic for $0.15 \leq x \leq 0.80$. The piezoelectric and dielectric response to an applied electric field was investigated, showing relaxor-like behavior for all materials. The maximum dielectric performance was observed for $x=0.15$ with $\epsilon'_{max} = 3507$ at $265^\circ C$ and the maximum converse piezoelectric performance was observed for $x=0.10$ with $S_{max}/E_{max} = 116$ pm/V. The functional properties in all show max performance in the composition region of phase transition from tetragonal to pseudo cubic crystal structure. This is in line with what has been observed for other BKT-based piezoelectrics, though not the best. The reported dielectric properties of the BKT-BNZ materials system demonstrated that the Ti-rich compositions show the highest performance. A tentative structural phase diagram for the reciprocal BKT-BNZ system was suggested

based on reported crystal symmetries and shows a large pseudo cubic region for intermediate compositions. Though the functional properties of BKT were improved by BNZ substitution, the BKT-BNZ composition joint does not provide lead-free alternatives to PZT.

Acknowledgements

Dr. Sverre Magnus Selbach is acknowledged for suggesting BKT-BNZ as a possible novel piezoelectric materials system. The Research Council of Norway (FRINATEK project no. 197497/F20) is acknowledged for financial support.

VI. Tables

Table 1: Optimized synthesis temperatures and subsequent sintered pellet relative density and grain size for the (1-x)BKT - xBNZ materials system.

Composition	Calcination	Sintering	Density, [%]	Grain size, [μm]
x = 0 (BKT)	700°C - 3 h	1060°C - 3 h	97 \pm 0.6	0.2 \pm 0.01
x = 0.05	700°C - 3 h	1050°C - 10 h	97 \pm 0.4	0.2 \pm 0.02
x = 0.10	700°C - 3 h	1050°C - 3 h	96 \pm 0.9	0.3 \pm 0.03
x = 0.15	700°C - 3 h	1050°C - 10 h	98 \pm 0.8	0.4 \pm 0.01
x = 0.20	700°C - 3 h	1050°C - 10 h	96 \pm 0.7	0.5 \pm 0.05
x = 0.30	750°C - 3 h	1000°C - 10 h	96 \pm 1	0.6 \pm 0.06
x = 0.40	750°C - 3 h	980°C - 10 h	96 \pm 0.7	2.0 \pm 0.1
x = 0.50	750°C - 3 h	980°C - 10 h	96 \pm 0.6	4.8 \pm 0.5
x = 0.60	750°C - 3 h	980°C - 10 h	92 \pm 2	-
x = 0.70	750°C - 3 h	980°C - 10 h	93 \pm 0.5	-
x = 0.80	750°C - 3 h	875°C - 3 h	96 \pm 0.5	-
x = 0.90	700-1050°C - 3 h	-	-	-
x = 1 (BNZ)	750°C - 3 h	850°C - 3 h	96 \pm 1	-

Table 2: Tabulated cell parameters, piezoelectric and dielectric data for the (1-x)BKT - xBNZ materials system.

Composition	Cell parameters, (Å)			P_{max}	$S_{max,b}$	$S_{max,u}/E_{max}$	ϵ'_{max}
	a	b	c	($\mu\text{C cm}^{-1}$)	(%)	(pm/V)	@ 10 kHz
x = 0 (BKT)	3.933(3)	-	3.975(4)	12	0.03	46	2575 (378°C)
x = 0.05	3.954(6)	-	3.962(8)	14	0.04	62	2954 (329°C)
x = 0.10	3.96(2)	-	3.96(2)	21	0.08	116	3296 (308°C)
x = 0.15	3.975(1)	-	-	13	0.04	61	3507 (265°C)
x = 0.20	3.9799(8)	-	-	14	0.04	61	2555 (243°C)
x = 0.30	4.0042(7)	-	-	10	0.02	36	1788 (212°C)
x = 0.40	4.0186(4)	-	-	7	0.01	16	1217 (232°C)
x = 0.50	4.0325(4)	-	-	4	0.01	9	906 (251°C)
x = 0.60	4.0416(3)	-	-	-	-	-	-
x = 0.70	4.0508(2)	-	-	-	-	-	-
x = 0.80	4.0585(3)	-	-	-	-	-	-
x = 1 (BNZ)	5.787(4)	8.162(5)	5.694(3)	-	-	-	-

VII. Figures

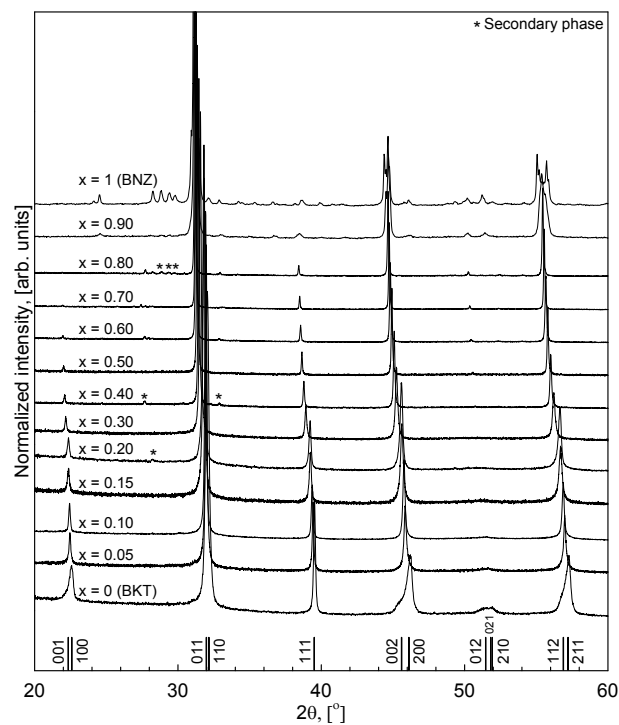


Figure 1: X-ray diffractograms of sintered compositions $(1-x)\text{BKT} - x\text{BNZ}$ ($x=0-1$). The intensity is normalized to the maximum intensity. The lower indices refer to tetragonal BKT.

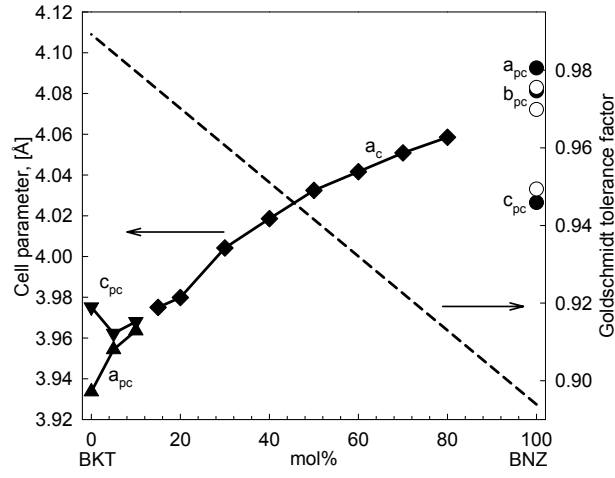


Figure 2: Pseudo cubic (a_{pc} , b_{pc} and c_{pc}) and cubic (a_c) unit cell parameters as a function of composition for (1-x)BKT - xBNZ ($x=0-0.8$). The orthorhombic unit cell parameters for $x=1.0$ are normalized as follows; $a_{pc}=2^{-1/2}a_{orth}$, $b_{pc}=0.5b_{orth}$ and $c_{pc}=2^{-1/2}c_{orth}$. Filled symbols from this work, open circles from elsewhere.²⁴ Also shown is the Goldschmidt tolerance factor (dashed line).³¹

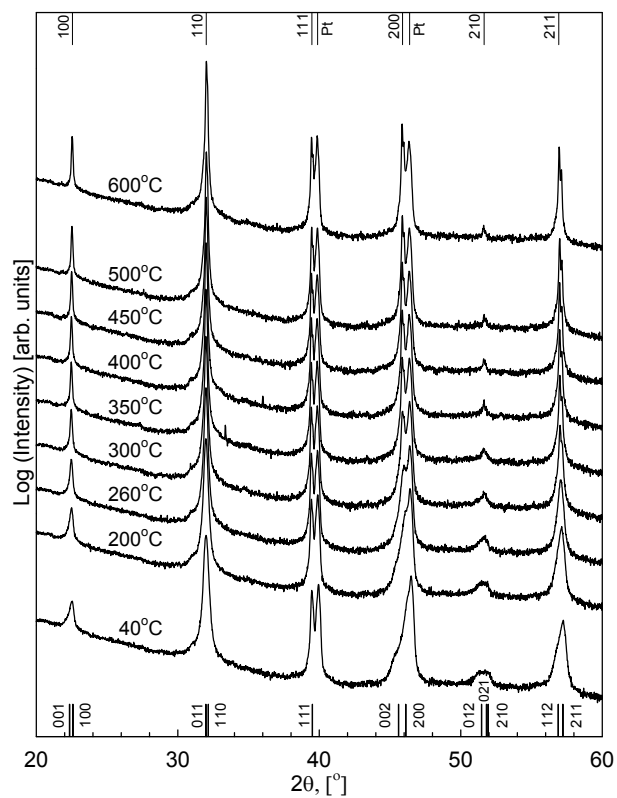


Figure 3: X-ray diffractograms for BKT ($x=0$) at selected temperatures. The lower indices refer to tetragonal BKT and upper indices to cubic BKT. Reflections due to platinum sample stage shown at $\sim 39.8^\circ$ and $\sim 46.3^\circ$.

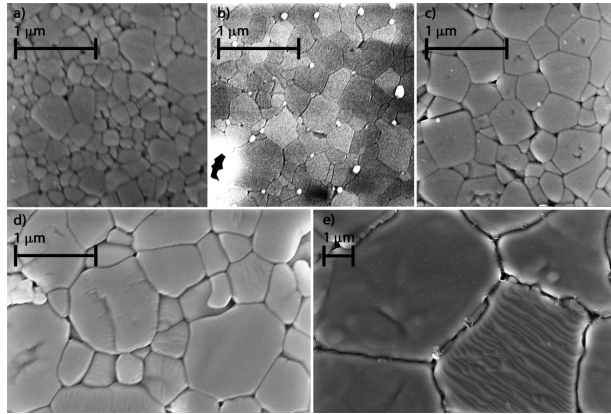


Figure 4: SEM micrographs of thermally etched pellet surfaces, a) BKT ($x=0$); b) 0.1BNZ; c) 0.15BNZ; d) 0.3BNZ; e) 0.5BNZ (note larger scale).

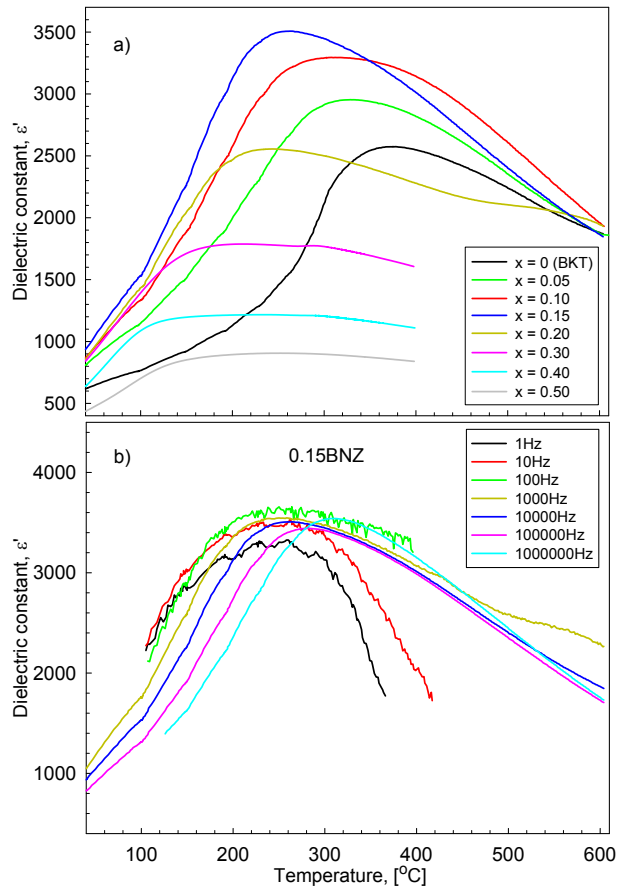


Figure 5: Temperature dependence of the dielectric constant for (1-x)BKT - xBNZ (x=0-0.5) at 10 kHz (a) and frequency and temperature dispersion of the dielectric permittivity of 0.15BNZ (b).

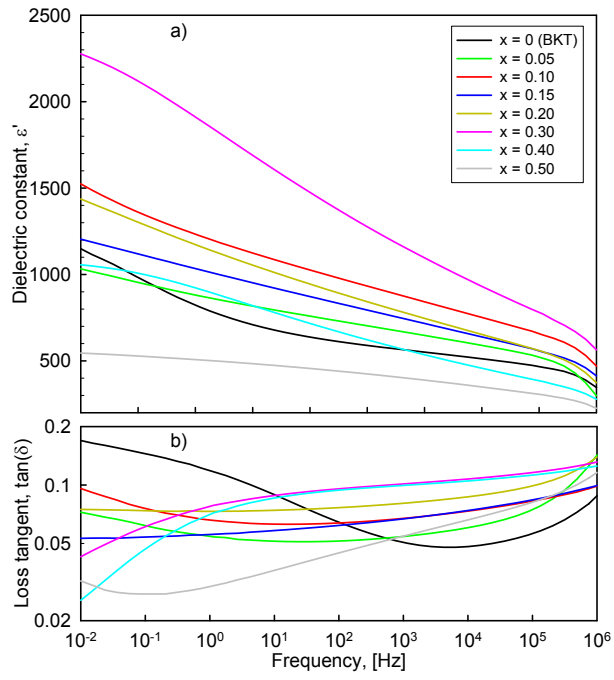


Figure 6: Room temperature dielectric constant (a) and loss (b) as a function of frequency of the samples used for electromechanical testing for $(1-x)\text{BKT} - x\text{BNZ}$ ($x=0-0.5$).

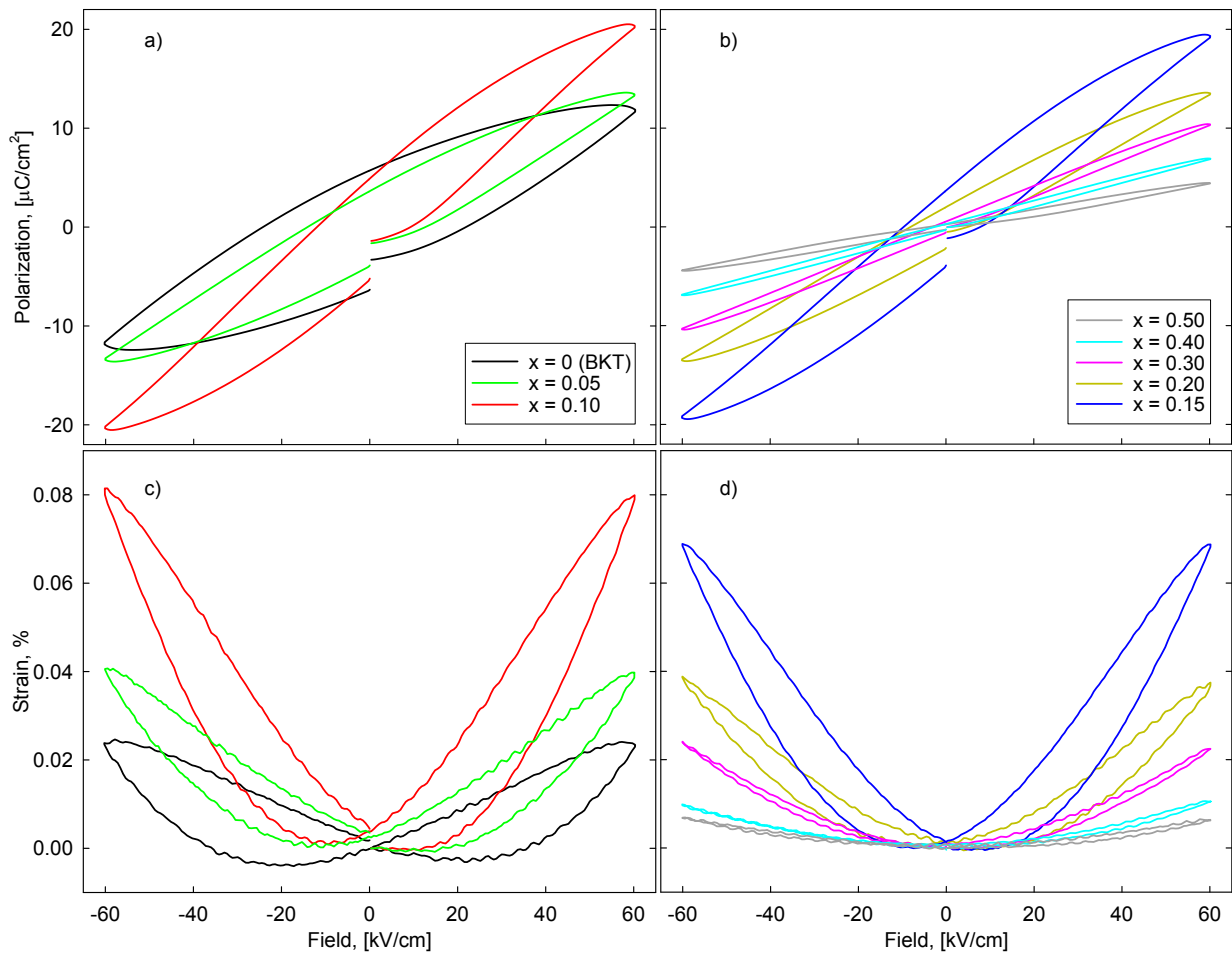


Figure 7: Bipolar polarization (a and b) and strain (c and d) for sintered ceramics of composition $(1-x)\text{BKT} - x\text{BNZ}$ ($x=0-0.5$).

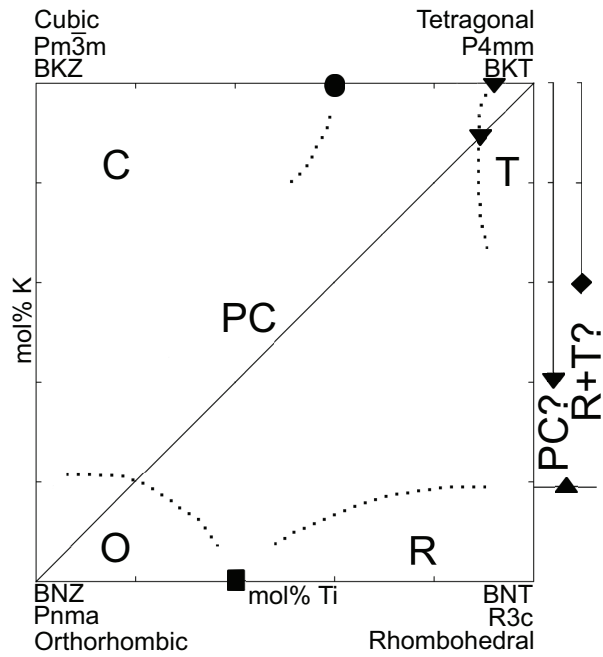


Figure 8: Tentative structural phase diagram in the ternary reciprocal system BKT-BNZ based on reported crystal symmetries. Solid marks along the binary joints represent reported phase transitions (PC = pseudo cubic); circle PC-C¹², triangle down T-PC^{12, 39} as reported by³³ and this work, diamond T-(R+T?)³², triangle up (PC?)/(R+T?)/T-R^{11,32} and³⁹ as reported by³³, and square R-O^{21,34}. Dotted lines possible phase dominance areas.

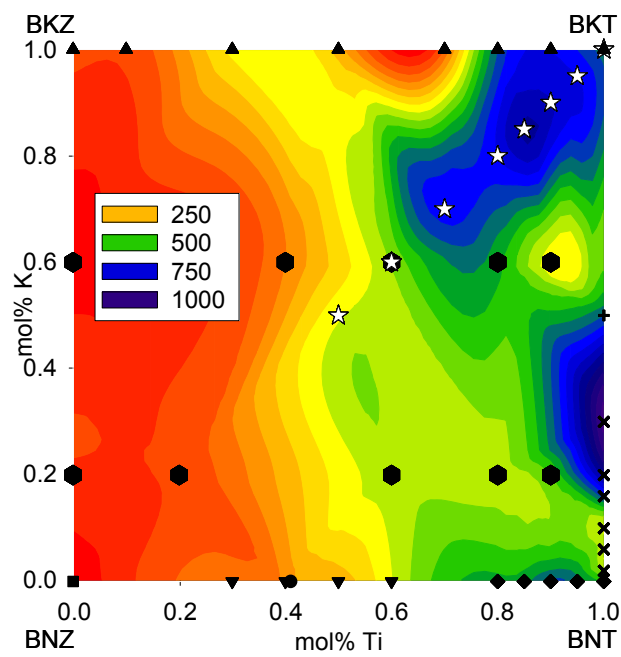


Figure 9: Contour plot of RT dielectric constants in the BKT-BNZ system. Data are gathered from the following literature (frequency = 10 kHz if not stated otherwise): stars (this work), triangle up¹², triangle down³⁴, hexagons (100 kHz)²¹, plus (1 MHz)³⁶, cross¹⁰, diamond²⁵, square⁴³, circle⁴⁴.

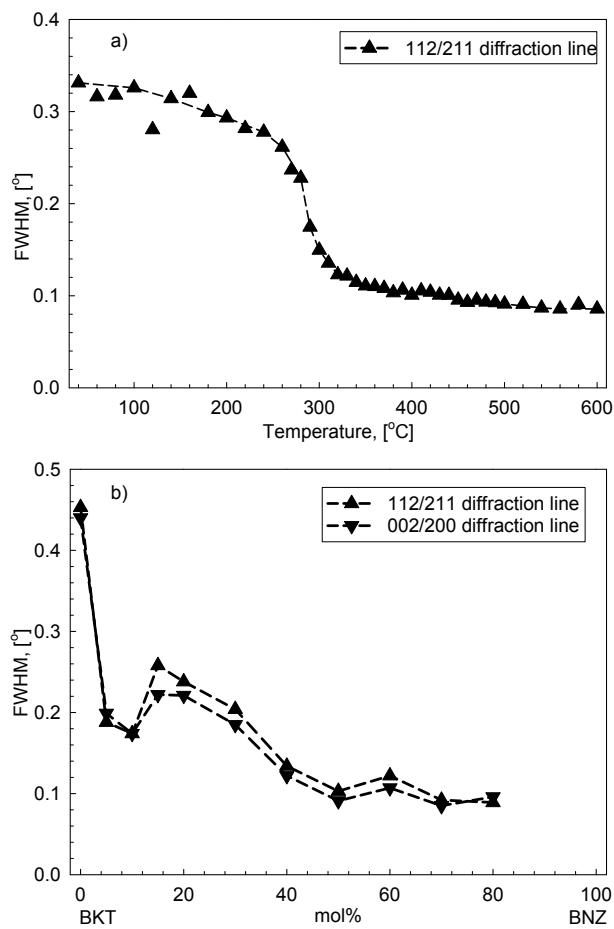


Figure 10: FWHM of the a); 112/211 XRD reflections as a function of temperature for BKT ($x=0$) and b); 112/211 and 002/200 XRD reflections as a function of composition of $(1-x)\text{BKT} - x\text{BNZ}$ ($x=0-0.8$). Dashed line added as guide to the eye.

1. J. Rödel, W. Jo, K. T. P. Seifert, E. M. Anton, T. Granzow, and D. Damjanovic, "Perspective on the development of lead-free piezoceramics," J. Am. Ceram. Soc. **92** [6] 1153–1177 (2009).
2. "EU-DIRECTIVE 2011/65/EU: Restriction of the use of certain hazardous substances in electrical and electronic equipment (RoHS)," Off. J. Eur. Union. **54** [L174] 89–110 (2011).
3. C. F. Buhner, "Some properties of bismuth perovskites," J. Chem. Phys. **36** [3] 798–803 (1962).
4. Y. Hiruma, H. Nagata, and T. Takenaka, "Grain-size effect on electrical properties of $\text{Bi}_{0.5}\text{K}_{0.5}\text{TiO}_3$ ceramics," Jpn. J. Appl. Phys. Pt. 1 **46** [3A] 1081–1084 (2007).
5. Y. Hiruma, R. Aoyagi, H. Nagata, and T. Takenaka, "Ferroelectric and piezoelectric properties of $\text{Bi}_{0.5}\text{K}_{0.5}\text{TiO}_3$ ceramics," Jpn. J. Appl. Phys. Pt. 1 **44** [7A] 5040–5044 (2005).
6. V. Dorcet, G. Trolliard, and P. Boullay, "Reinvestigation of phase transitions in $\text{Na}_{0.5}\text{Bi}_{0.5}\text{TiO}_3$ by TEM. Part I: First order rhombohedral to orthorhombic phase transition," Chem. Mater. **20** [15] 5061–5073 (2008).
7. G. Trolliard and V. Dorcet, "Reinvestigation of phase transitions in $\text{Na}_{0.5}\text{Bi}_{0.5}\text{TiO}_3$ by TEM. Part II: Second order orthorhombic to tetragonal phase transition," Chem. Mater. **20** [15] 5074–5082 (2008).
8. V. V. Ivanova, A. G. Kapyshev, Y. N. Venevtsev, and G. S. Zhdanov, Izv. Akad. Nauk. SSSR. **26** 354 (1962).
9. G. A. Smolenskii, V. A. Isupov, A. I. Agranovskaya, and N. N. Krainik, "New ferroelectrics of complex composition IV," Sov. Phys. - Solid State **2** [11] 2651–2654 (1961).
10. Y. Hiruma, K. Yoshii, H. Nagata, and T. Takenaka, "Phase transition temperature and electrical properties of $(\text{Bi}_{0.5}\text{Na}_{0.5})\text{TiO}_3$ - $(\text{Bi}_{0.5}\text{A}_{0.5})\text{TiO}_3$ (A=Li and K) lead-free ferroelectric ceramics," J. Appl. Phys. **103** [8] 084121 7pp. (2008).
11. A. Sasaki, T. Chiba, Y. Mamiya, and E. Otsuki, "Dielectric and piezoelectric properties of $(\text{Bi}_{0.5}\text{Na}_{0.5})\text{TiO}_3$ - $(\text{Bi}_{0.5}\text{K}_{0.5})\text{TiO}_3$ systems," Jpn. J. Appl. Phys. Pt. 1 **38** [9B] 5564–5567 (1999).
12. M. Bengagi, F. Morini, M. El Maaoui, and P. Marchet, "Structure and electrical properties in the $\text{K}_{0.5}\text{Bi}_{0.5}\text{TiO}_3$ - $\text{K}_{0.5}\text{Bi}_{0.5}\text{ZrO}_3$ solid solution (KBT-KBZ)," Phys. Status Solidi A **209** [10] 2063–2072 (2012).
13. M. I. Morozov, M.-A. Einarsrud, and T. Grande, "Polarization and strain response in $\text{Bi}_{0.5}\text{K}_{0.5}\text{TiO}_3$ - BiFeO_3 ceramics," Appl. Phys. Lett. **101** [25] 252904 4pp. (2012).
14. M. I. Morozov, M.-A. Einarsrud, T. Grande, and D. Damjanovic, "Lead-free relaxor-like $0.75\text{Bi}_{0.5}\text{K}_{0.5}\text{TiO}_3$ - 0.25BiFeO_3 ceramics with large electric field-induced strain," Ferroelectrics **439** [1] 88–94 (2012).
15. Y. Hiruma, R. Aoyagi, H. Nagata, and T. Takenaka, "Piezoelectric properties of BaTiO_3 - $(\text{Bi}_{0.5}\text{K}_{0.5})\text{TiO}_3$ ferroelectric ceramics," Jpn. J. Appl. Phys. Pt. 1 **43** [11A] 7556–7559 (2004).
16. H. L. Du, W. C. Zhou, F. Luo, D. M. Zhu, S. B. Qu, Y. Li, and Z. B. Pei, "Polymorphic phase transition dependence of piezoelectric properties in $(\text{K}_{0.5}\text{Na}_{0.5})\text{NbO}_3$ - $(\text{Bi}_{0.5}\text{K}_{0.5})\text{TiO}_3$ lead-free ceramics," J. Phys. D: Appl. Phys. **41** [11] 115413 5pp. (2008).
17. L. Martin-Arias, A. Castro, and M. Alguero, "Ferroelectric phases and relaxor states in the novel lead-free $(1-x)$ $(\text{Bi}_{0.5}\text{K}_{0.5})\text{TiO}_3$ - x BiScO_3 system ($0 \leq x \leq 0.3$)," J. Mater. Sci. **47** [8] 3729–3740 (2012).
18. T. Takenaka, K. Maruyama, and K. Sakata, " $(\text{Bi}_{0.5}\text{Na}_{0.5})\text{TiO}_3$ - BaTiO_3 system for lead-free piezoelectric ceramics," Jpn. J. Appl. Phys. Pt. 1 **30** [9B] 2236–2239 (1991).
19. R. Z. Zuo, X. S. Fang, and C. Ye, "Phase structures and electrical properties of new lead-free $(\text{Na}_{0.5}\text{K}_{0.5})\text{NbO}_3$ - $(\text{Bi}_{0.5}\text{Na}_{0.5})\text{TiO}_3$ ceramics," Appl. Phys. Lett. **90** [9] 092904 3pp. (2007).
20. T. Takenaka, T. Okuda, and K. Takegahara, "Lead-free piezoelectric ceramics based on $(\text{Bi}_{0.5}\text{Na}_{0.5})\text{TiO}_3$ - NaNbO_3 ," Ferroelectrics **196** [1-4] 495–498 (1997).
21. Y. Yamada, T. Akutsu, H. Asada, K. Nozawa, S. Hachiga, T. Kurosaki, O. Ikagawa, H. Fujiki, et al., "Effect of B-ions

- substitution in $[(K_{0.5}Bi_{0.5})-(Na_{0.5}Bi_{0.5})](Ti-B)O_3$ system with $B = Zr, Fe_{1/2}Nb_{1/2}, Zn_{1/3}Nb_{2/3}$ or $Mg_{1/3}Nb_{2/3}$,” Jpn. J. Appl. Phys. Pt. 1 **34** [9B] 5462–5466 (1995).
22. A. Rachakom, P. Jaiban, S. Jiansirisomboon, and A. Watcharapasorn, “Crystal structure and electrical properties of bismuth sodium titanate zirconate ceramics,” Nanoscale. Res. Lett. **7** 57 5pp. (2012).
 23. L. Kumari, K. Kumari, K. Prasad, and R. N. P. Choudhary, “Impedance spectroscopy of $(Na_{0.5}Bi_{0.5})(Zr_{0.25}Ti_{0.75})O_3$ lead-free ceramic,” J. Alloy. Compd. **453** [1-2] 325–331 (2008).
 24. P. Jaiban, A. Rachakom, S. Buntham, S. Jiansirisomboon, and A. Watcharapasorn, “Fabrication of $Bi_{0.5}Na_{0.5}ZrO_3$ powder by mixed oxide method,” Mater. Sci. Forum **695** 49–52 (2011).
 25. A. Watcharapasorn and S. Jiansirisomboon, “Dielectric and piezoelectric properties of zirconium-doped bismuth sodium titanate ceramics,” Adv. Mat. Res. **55-57** 133–136 (2008).
 26. D. A. Berlincourt, C. Cmolik, and H. Jaffe, “Piezoelectric properties of polycrystalline lead titanate zirconate compositions,” P. IRE. **48** [2] 220–229 (1960).
 27. N. Zhang, H. Yokota, A. M. Glazer, and P. A. Thomas, “Neutron powder diffraction refinement of $PbZr_{1-x}Ti_xO_3$,” Acta Cryst. B **67** [5] 386–398 (2011).
 28. Bruker AXS, “Topas,” Version 4.2 (2009), URL www.bruker-axs.com.
 29. S. L. Sorokina and A. W. Sleight, “New phases in the ZrO_2 - Bi_2O_3 and HfO_2 - Bi_2O_3 systems,” Mater. Res. Bull. **33** [7] 1077–1081 (1998).
 30. M. Otoničar, S. D. Škapin, B. Jančar, R. Ubič, and D. Suvorov, “Analysis of the phase transition and the domain structure in $K_{0.5}Bi_{0.5}TiO_3$ perovskite ceramics by In Situ XRD and TEM,” J. Am. Ceram. Soc. **93** [12] 4168–4173 (2010).
 31. R. D. Shannon, “Revised effective ionic-radii and systematic studies of interatomic distances in halides and chalcogenides,” Acta Crystallogr., Sect. A: Found. Crystallogr. **32** [SEP1] 751–767 (1976).
 32. O. Elkechai, M. Manier, and J. P. Mercurio, “ $Na_{0.5}Bi_{0.5}TiO_3$ - $K_{0.5}Bi_{0.5}TiO_3$ (NBT-KBT) system: A structural and electrical study,” Phys. Status Solidi A **157** [2] 499–506 (1996).
 33. J. Kreisel, A. M. Glazer, G. Jones, P. A. Thomas, L. Abello, and G. Lucazeau, “An x-ray diffraction and Raman spectroscopy investigation of A-site substituted perovskite compounds: the $(Na_{1-x}K_x)_{0.5}Bi_{0.5}TiO_3$ ($0 \leq x \leq 1$) solid solution,” J. Phys.: Condens. Matter. **12** [14] 3267–3280 (2000).
 34. P. Jaiban, A. Rachakom, S. Jiansirisomboon, and A. Watcharapasorn, “Influences of phase transition and microstructure on dielectric properties of $Bi_{0.5}Na_{0.5}Zr_{1-x}Ti_xO_3$ ceramics,” Nanoscale Res. Lett. **7** [1] 45 5pp. (2012).
 35. A. A. Bokov and Z.-G. Ye, “Recent progress in relaxor ferroelectrics with perovskite structure,” J. Mater. Sci. **41** [1] 31–52 (2006).
 36. M. Otoničar, S. D. Škapin, M. Spreitzer, and D. Suvorov, “Compositional range and electrical properties of the morphotropic phase boundary in the $Na_{0.5}Bi_{0.5}TiO_3$ - $K_{0.5}Bi_{0.5}TiO_3$ system,” J. Eur. Ceram. Soc. **30** [4] 971–979 (2010).
 37. T. Wada, A. Fukui, and Y. Matsuo, “Preparation of $(K_{0.5}Bi_{0.5})TiO_3$ ceramics by polymerized complex method and their properties,” Jpn. J. Appl. Phys. Pt. 1 **41** [11B] 7025–7028 (2002).
 38. V. A. Shuvaeva, D. Zekria, A. M. Glazer, Q. Jiang, S. M. Weber, P. Bhattacharya, and P. A. Thomas, “Local structure of the lead-free relaxor ferroelectric $(K_xNa_{1-x})_{0.5}Bi_{0.5}TiO_3$,” Phys. Rev. B **71** [17] 174114 8pp. (2005).
 39. I. P. Pronin, N. N. Parfenova, N. V. Zaitseva, V. A. Isupov, and G. A. Smolenskii, Sov. Phys.-Solid State **24** 1060–1062 (1982).
 40. A. B. Kounga, S. T. Zhang, W. Jo, T. Granzow, and J. Rodel, “Morphotropic phase boundary in $(1-x)Bi_{0.5}Na_{0.5}TiO_3$ - $xK_{0.5}Na_{0.5}NbO_3$ lead-free piezoceramics,” Appl Phys Lett **92** [22] 222902 3pp. (2008).
 41. J. F. Scott, “Ferroelectrics go bananas,” J. Phys.-Condens. Mat. **20** [2] 021001 2pp. (2008).

42. A. Reisman, "Heterogeneous equilibria in the system K_2CO_3 - Na_2CO_3 ," *J. Am. Chem. Soc.* **81** [4] 807–811 (1959).
43. Lily, K. Kumari, K. Prasad, and K. L. Yadav, "Dielectric and impedance study of lead-free ceramic: $(Na_{0.5}Bi_{0.5})ZrO_3$," *J. Mater. Sci.* **42** [15] 6252–6259 (2007).
44. P. Jaiban, S. Jiansirisomboon, and A. Watcharapasorn, "Effect of lanthanum substitution on microstructure and electrical properties of $(Bi_{0.5}Na_{0.5})_{1-1.5x}La_xTi_{0.41}Zr_{0.59}O_3$ ceramics," *Ceram. Int.* **38** S379–S383 (2012).

VIII. Figure captions

Figure 1: X-ray diffractograms of sintered compositions (1-x)BKT - xBNZ (x=0-1). The intensity is normalized to the maximum intensity. The lower indices refer to tetragonal BKT.

Figure 2: Pseudo cubic (a_{pc} , b_{pc} and c_{pc}) and cubic (a_c) unit cell parameters as a function of composition for (1-x)BKT - xBNZ (x=0-0.8). The orthorhombic unit cell parameters for x=1.0 are normalized as follows; $a_{pc}=2^{-1/2}a_{orth}$, $b_{pc}=0.5b_{orth}$ and $c_{pc}=2^{-1/2}c_{orth}$. Filled symbols from this work, open circles from elsewhere.²⁴ Also shown is the Goldschmidt tolerance factor (dashed line).³¹

Figure 3: X-ray diffractograms for BKT (x=0) at selected temperatures. The lower indices refer to tetragonal BKT and upper indices to cubic BKT. Reflections due to platinum sample stage shown at $\sim 39.8^\circ$ and $\sim 46.3^\circ$.

Figure 4: SEM micrographs of thermally etched pellet surfaces, a) BKT (x=0); b) 0.1BNZ; c) 0.15BNZ; d) 0.3BNZ; e) 0.5BNZ (note larger scale).

Figure 5: Temperature dependence of the dielectric constant for (1-x)BKT - xBNZ (x=0-0.5) at 10 kHz (a) and frequency and temperature dispersion of the dielectric permittivity of 0.15BNZ (b).

Figure 6: Room temperature dielectric constant (a) and loss (b) as a function of frequency of the samples used for electromechanical testing for (1-x)BKT - xBNZ (x=0-0.5).

Figure 7: Bipolar polarization (a and b) and strain (c and d) for sintered ceramics of composition (1-x)BKT - xBNZ (x=0-0.5).

Figure 8: Tentative structural phase diagram in the ternary reciprocal system BKT-BNZ based on reported crystal symmetries. Solid marks along the binary joints represent reported phase transitions (PC = pseudo cubic); circle PC-C¹², triangle down T-PC^{12, 39} as reported by³³ and this work, diamond T-(R+T?)³², triangle up (PC?)/(R+T?)/T-R^{11, 32} and³⁹ as reported by³³, and square R-O^{21, 34}. Dotted lines possible phase dominance areas.

Figure 9: Contour plot of RT dielectric constants in the BKT-BNZ system. Data are gathered from the following literature (frequency = 10 kHz if not stated otherwise): stars (this work), triangle up¹², triangle down³⁴, hexagons (100 kHz)²¹, plus (1 MHz)³⁶, cross¹⁰, diamond²⁵, square⁴³, circle⁴⁴.

Figure 10: FWHM of the a); 112/211 XRD reflections as a function of temperature for BKT (x=0) and b); 112/211 and 002/200 XRD reflections as a function of composition of (1-x)BKT - XBNZ (x=0-0.8). Dashed line added as guide to the eye.